Multimed Tools Appl manuscript No.
(will be inserted by the editor)

A novel forensic image analysis tool for discovering double JPEG compression clues

Ali Taimori · Farbod Razzazi · Alireza Behrad · Ali Ahmadi · Massoud Babaie-Zadeh

Received: date / Accepted: date

Abstract This paper presents a novel technique to discover double JPEG compression traces. Existing detectors only operate in a scenario that the image under investigation is explicitly available in JPEG format. Consequently, if quantization information of JPEG files is unknown, their performance dramatically degrades. Our method addresses both forensic scenarios which results in a fresh perceptual detection pipeline. We suggest a dimensionality reduction algorithm to visualize behaviors of a big database including various single and double compressed images. Based on intuitions of visualization, three bottom-up, top-down and combined top-down/bottom-up learning strategies are proposed. Our tool discriminates single compressed images from double counterparts, estimates the first quantization in double compression, and localizes tampered regions in a forgery examination. Extensive experiments on three databases demonstrate results are robust among different quality levels.

Ali Taimori
Young Researchers and Elite Club, Parand Branch, Islamic Azad University, Parand, Iran
E-mail: alitaimori@yahoo.com

Farbod Razzazi
Department of Electrical and Computer Engineering, Science and Research Branch, Islamic Azad University, Tehran 14778-93855, Iran
E-mail: razzazi@srbiau.ac.ir

Alireza Behrad
Faculty of Engineering, Shahed University, Tehran 18651-33191, Iran
E-mail: behrad@shahed.ac.ir

Ali Ahmadi
Department of Electrical and Computer Engineering, K. N. Toosi University of Technology, Tehran 14317-14191, Iran
E-mail: ahmadi@eetd.kntu.ac.ir

Massoud Babaie-Zadeh
Department of Electrical Engineering, Sharif University of Technology, Tehran 14588-89694, Iran
E-mail: mbzadeh@sharif.edu

F_1-measure improvement to the best state-of-the-art approach reaches up to 26.32%. An implementation of algorithms is available upon request to fellows.

Keywords Compressive sensing · dimensionality reduction · double compression detection · forgery locating · recompression history identification · top-down and bottom-up processing.

1 Introduction

In the digital era, the deployment of image acquisition devices has caused widespread use and share of images in cyberspace. On the other hand, due to the advancement of image processing tools, we have several powerful image editing software packages now. Unfortunately, forgers misuse such a scientific progress, so that the integrity of digital images is nowadays doubtful for governments, the police, courts of justice, journalists, universities, people and the whole society. Emerging technology of image forensics offers active and passive techniques to cope with this problem [36].

Passive approaches exploit statistical and intrinsic characteristics of digital images as the legal evidence which assist forensic analysts to decide about their authenticity [30]. In this context, one of interesting investigations is to discover intrinsic signatures of Joint Photographic Experts Group (JPEG) images that are widely employed by most digital cameras. As a real scenario of JPEG image manipulation, consider the case in which a photographic forger opens a JPEG image in a photo-editing software package and after some invisible alterations saves it again in the same well-known default format. In the digital forensics community, such a manipulation process is called double compression [11, 35]. The present paper deals with this enquiry and introduces a new forensic tool for the detection of double JPEG compression, the identification of recompression history and the localization of forged regions in images to be able to discriminate between original images and tampered contents.

1.1 Forensic scenarios

In the problem of Double JPEG Compression Detection (DJCD), this paper addresses two important forensic scenarios as follows. As the first scenario, if the image under investigation is available in JPEG format, the last compression history, embedded in JPEG metadata, is known. It can be accessible by reading the coder information in JPEG file stream. Note that, in this case, the primary compression history such as the quantization table is unknown for a doubly compressed JPEG image. We refer to the problem in such a scenario as "quantization-semi-aware DJCD". This well-known scenario has been investigated by several researchers in the literature [7, 18, 31, 42]. Generally, in the quantization-semi-aware DJCD, several learned models may be employed to cover all possible compression's quality levels that this matter requires a long time and a great memory for examining suspect images.

As the second scenario, if the image under analysis is not explicitly available in JPEG format, the first and last quantization tables information of a doubly compressed image are unknown [42]. This fact makes it much more challenging than the traditional first scenario. We call such a forensic scenario as "quantization-unaware DJCD". The quantization-unaware double compression detection can be forensically important for some reasons as follows.

- It is forensically valuable to identify recompression history of a decoded double compressed JPEG image that is resaved in an uncompressed form like the bitmap (BMP) image.
- Situations in which the embedded JPEG metadata is not reliably identifiable, due to noise in a transmission channel or other jamming factors.
- The quantization table of a JPEG metadata is missing of its header file [37].
- As an alternative solution of detecting double compression, in the quantization-unaware DJCD, only one learned model may be exploited to save time and memory.

1.2 Related arts

As mentioned, for detecting quantization-semi-aware double JPEG compression, different approaches have been proposed [7, 18, 31, 42]. B. Li et al. [18] presented an algorithm for detecting double compression and estimating the primary compression quality level based on the first digit features of individual Alternating Current (AC) modes. Their seminal paper was a basis for developing several methods like [7, 19, 31]. For instance, in [31], Milani et al. improved the accuracy of [18] by a feature selection mechanism to be able to identify recompression stages up to four times. In another study, to detect double compression, Dong et al. [7] leveraged inter-block correlation of quantized Discrete Cosine Transform (DCT) coefficients via Markov model of leading digits from individual AC modes. By considering these inconsistencies, their approach had only a modest improvement for a few quality levels compared to the method [18].

Image manipulation techniques may have various forms [11, 30]. Due to this fact, different methods exist to detect image forgery including pixel-, statistics-, format-, camera- and physics- based approaches, and geometric methods [11]. In [30], Mahalakshmi et al. proposed algorithms for detecting basic image processing operations like rotation, rescaling, contrast enhancement and histogram equalization that are frequently used in image retouching. Format-based methods deal with the image compression artifacts to discover tampering. Here, we address the problem of locating tampered regions in the presence of double JPEG compression. For instance, X. H. Li et al. suggested an image forgery detection algorithm [19], which gains the Benford-based feature extraction approach presented in [18] to improve the performance of the saliency map-based tampering detector of [22].

In the forensic investigation of a JPEG file, the identification of its quantization history may expose information about the device that has been captured the image under analysis. Such a procedure has so-called "digital image ballistics" in [10]. This imprint may be achieved by estimating the primary quality level or its corresponding quantization table of a doubly compressed JPEG image [3, 12, 18, 26, 34]. Bianchi and Piva [3] estimated the first quantization steps separately for each frequency mode and localized forged regions in a double compressed JPEG image based on the Expectation Maximization (EM) algorithm and a likelihood map stemmed from the Bayesian modeling. Based on the DCT grid alignment of the first compression with the second one, this method takes into account the traces left by both aligned and nonaligned DCT grid. But, their algorithm cannot appropriately detect the original un-manipulated single compressed images captured by cameras. Additionally, their DJCD modeling is affected by the estimation performance of the primary quantization table. By applying a DCT histogram filtering and defining an error function, Galvan et al. [12] improved the performance of the first quantization table estimation on the algorithm [3] in double compressed images merely when $l_1 < l_2$ (Hereafter, l_1 and l_2 represent the quality level or factor in the first and second compression, respectively. In the baseline JPEG compression which is concerned with scientific research of forensic examiners [3, 7, 12, 18, 19, 22, 24, 26, 31, 34, 42], there exist $1 \leqslant l_1, l_2 \leqslant 100$.). However, in more challenging cases, i.e. $l_1 > l_2$ and $l_1 = l_2$, their approach has not been assessed, whereas the method [3] deals with all aforementioned quality level settings.

1.3 Motivations and contributions

Most previous arts suffer from unsatisfactory performance when $l_1 \geqslant l_2$. In addition, they can only be effective for the quantization-semi-aware scenario of DJCD rather than the unknown-quantization table case. Forgery localization methods, like the algorithm [3], cannot also decide about the authenticity of original un-manipulated images captured by digital cameras. In contrast, the present study is able to discriminate single compressed images from double compressed ones for both quantization- unaware and semi-aware scenarios as well as localize tampered regions of actual forged images.

In order to estimate the first quantization matrix, the methods [3, 12, 18] rely on the assumption for which the image under investigation is doubly compressed; whereas the proposed method identifies both Single/Double (S/D) compression and the first quality level from double compressed images in one step and without the mentioned presumption. Additionally, the approaches such as [3, 12, 26] are inaccurate to estimate high frequency quantization steps of the first quantization table pertaining to a given JPEG coder. Whereas different image encoders leave distinct forensic traces that can be exploited to identify their origin [21]. However, the methods [3, 12] did not gain these discriminative information. It is possible to strongly improve their estimation

performance by leveraging the coder's behavior. To this intent, Peng and Liu [34] moved a step forward in identifying the whole primary quantization matrix accurately. They derived a statistical model which takes into account the correlation between the first and second compression. In this regard, our primary quality level estimator can robustly discover the whole quantization table in the challenging quality level settings. Briefly, in coping with the above mentioned problems, we propose a new DJCD method with the following benefits.

- Without knowing quantization information, the method can detect double JPEG compressed images.
- The method is able to accurately estimate the secondary compression's quality level as well as its corresponding quantization table of doubly compressed images in the quantization-unaware scenario.
- The method is able to estimate the compression's quality level as well as its corresponding quantization table of singly compressed images in the quantization-unaware scenario.
- The method can robustly detect double compressed images in both $l_1 > l_2$ and $l_1 < l_2$ cases (i.e. when $l_1 \neq l_2$).
- The suggested approach can be employed to identify bitmap recompression history.
- For the quantization-unaware scenario, the proposed method only uses two learned models to predict double JPEG compression and does not need many individual trained models.
- Our method can be exploited in a sub-image filtering manner to locate altered regions of tampered images.

The methods presented in the literature [3, 7, 12, 18, 19, 22, 24, 31, 41, 42] did not consider intra-category variations to detect double compression. In contrast, we first generated a statistical hypothesis that JPEG compressed images with varying compression's quality factor have distinctive clusters in the feature space. Then, we validated this hypothesis by a feature visualizer technique. The proposed algorithm stems from a suggested big data analysis on various single and double compressed images of a given database with different compression's quality levels. In this way, we proposed a novel Dimensionality Reduction (DR) method to visualize the behavior of these data in the 2-Dimensional (2-D) scatterplot. The visualized information of the JPEG coder was a basis for constructing a Bottom-Up (BU) learning strategy which can take into account local structures of data. In order to get a global insight into the single and double compression groups, we also suggested a complement Top-Down (TD) learner system.

Recently, merged TD and BU schemes, in a general sense, have been successfully demonstrated in some data processing tasks, like saliency detection [43], image segmentation [4, 17] and speaker diarization [9]. Here, due to the complementarity nature of our TD and BU learning strategies, we designed a novel combined perceptual top-down/bottom-up approach to reliably detect double compression for both quantization- unaware and semi-aware scenarios. We will describe that the idea behind the proposed approaches is close to hu-

man perception system. In a filtering mechanism, we show how the proposed algorithm can be employed to localize tampered regions in the forged images. Additionally, the suggested bottom-up approach accurately estimates the first quantization table from doubly compressed images. For reproducibility of the results, an implementation of our algorithms and the used image-sets are available upon request to fellow researchers. Considering both quantization-unaware and semi-aware scenarios, at a glance, the main contributions of this paper are

- proposing an information visualization technique for analyzing the behavior of S/D compression in JPEG images which can be generalized to other image compression standards for identifying recompression clues,
- suggesting a learning-based bottom-up approach to accurately estimate the whole quantization steps of the first quantization matrix as well as detect double compression,
- introducing a combined perceptual top-down/bottom-up learning strategy for robust DJCD with respect to various $l_1 \neq l_2$ choices,
- proposing a sliding-window detector algorithm to localize forged regions in actual forensic investigations.

1.4 Paper organization

The remainder of this paper is organized as follows. Section 2 describes the proposed scheme. In this section, at first, we visualize the behavior of a given big database consisting of various single and double compressed images with different compression's quality level settings. Then, our visualizer establishes the basis of the proposed bottom-up, top-down and combined top-down/bottom-up learning strategies for forensic purposes of the first quality level estimation, double compression detection and forgery localization. In Section 3, we extensively assess the effectiveness of the suggested method from different aspects. Finally, the paper is discussed and concluded in Section 4.

2 Proposed approach

In this section, we first introduce an information visualizer technique in the 2-D feature space. This visualizer stems from a dedicated features' dimensionality reduction for analyzing the behavior of various singly and doubly compressed JPEG images with different compression's quality factors. To design the proposed scheme, we extract a set of features based on Benford's law [2, 41, 42] as initial feature vectors, which exploits all AC frequency modes. Starting from the intuitions of visualization, we then propose three models called bottom-up, top-down and combined top-down/bottom-up learning strategies as useful forensic techniques for estimating the first quantization table, detecting double JPEG compression and locating real image forgery. In the proposed method, we take into account both quantization- unaware and semi-aware scenarios.

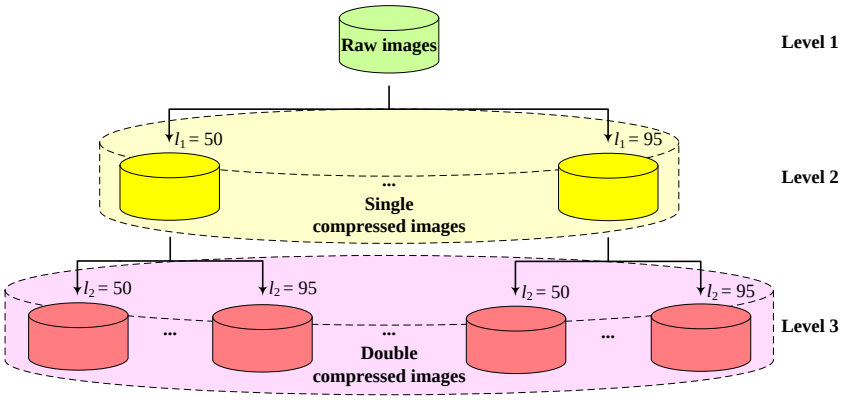

Fig. 1: The process of creating single and double compressed JPEG image patches. The parameters l_1 and l_2 represent the first and second compression's quality levels.

2.1 Visualization for identifying double compression clues

Here, different from previous arts, we accurately inspect the issue of double JPEG compression detection from a big-data analysis viewpoint. In this context, a statistical data analysis of single and double compressed image patches and their visualization in the 2-D scatterplot generate values to cope with such an issue.

2.1.1 Singly and doubly compressed image-sets

To provide single and double compressed JPEG image patches in simulations, consider a given database of raw images. At first, we compress each raw image of the database with the first quality level $l_1 \in \mathcal{Q}$ in JPEG format, which $\mathcal{Q} \triangleq \{50, 55, \ldots, 95\}$ for convenience. This set is frequently used in JPEG images and by digital forensic researchers [3, 7, 12, 18, 19, 22, 24, 26, 31, 42]. Although experimentation with lower compression's quality levels as well as the smaller step size is possible at the expense of more computation time, it deems to be sufficient based on the ergodicity principle to demonstrate our findings and compare it to the state-of-the-art approaches[1]. This process produces $|\mathcal{Q}| = 10$ different types or individual databases of singly compressed images which are grouped together to create the "single compressed images" database, as depicted at the second level of Fig. 1 (The symbol $|\cdot|$ represents the cardinality of a set.).

[1] In simple language, the ergodicity principle refers to the proverb "You may know by a handful the whole sack.".

Table 1: Definition 1 for different single and double compression groups and classes. G_1 and G_2 denote single and double compression groups, respectively. The single and double compression groups encompass the classes C_1 to C_{10}, and C_{11} to C_{110}, respectively.

G_2		l_1									
		50	55	60	65	70	75	80	85	90	95
l_2	50	C_{11}	C_{21}	C_{31}	C_{41}	C_{51}	C_{61}	C_{71}	C_{81}	C_{91}	C_{101}
	55	C_{12}	C_{22}	C_{32}	C_{42}	C_{52}	C_{62}	C_{72}	C_{82}	C_{92}	C_{102}
	60	C_{13}	C_{23}	C_{33}	C_{43}	C_{53}	C_{63}	C_{73}	C_{83}	C_{93}	C_{103}
	65	C_{14}	C_{24}	C_{34}	C_{44}	C_{54}	C_{64}	C_{74}	C_{84}	C_{94}	C_{104}
	70	C_{15}	C_{25}	C_{35}	C_{45}	C_{55}	C_{65}	C_{75}	C_{85}	C_{95}	C_{105}
	75	C_{16}	C_{26}	C_{36}	C_{46}	C_{56}	C_{66}	C_{76}	C_{86}	C_{96}	C_{106}
	80	C_{17}	C_{27}	C_{37}	C_{47}	C_{57}	C_{67}	C_{77}	C_{87}	C_{97}	C_{107}
	85	C_{18}	C_{28}	C_{38}	C_{48}	C_{58}	C_{68}	C_{78}	C_{88}	C_{98}	C_{108}
	90	C_{19}	C_{29}	C_{39}	C_{49}	C_{59}	C_{69}	C_{79}	C_{89}	C_{99}	C_{109}
	95	C_{20}	C_{30}	C_{40}	C_{50}	C_{60}	C_{70}	C_{80}	C_{90}	C_{100}	C_{110}
G_1		C_1	C_2	C_3	C_4	C_5	C_6	C_7	C_8	C_9	C_{10}

Then, each single compressed image of the above individual databases is compressed again with the second quality level $l_2 \in \mathcal{Q}$, achieving $|\mathcal{Q}| \times |\mathcal{Q}| = 100$ different types of doubly compressed JPEG images which are grouped together to create the "double compressed images" database, as shown at the third level of Fig. 1. As it can be seen in Fig. 1, the process of gathering S/D compressed data produces a big image database consisting of different types from both singly and doubly compressed JPEG images.

Definition 1 (S/D compression groups and classes) Suppose that $l_1, l_2 \in \mathcal{Q}$ are the first and second compression's quality levels in JPEG coder, respectively. Consider $\mathcal{Q} \triangleq \{50,\ 55,\ \ldots, 95\}$ for simplicity. If G_1 and G_2 respectively denote single and double compression groups, then, Table 1 defines single and double compression classes, in which $C_k,\ \forall k \in [1,\ N_c]$, represents the k^{th} class. By definition, we have $N_c = |\mathcal{Q}| + |\mathcal{Q}| \times |\mathcal{Q}| = 110$ classes.

2.1.2 Feature extraction

For visualizing and discovering knowledge, at first, we extract informative features from different types of single and double compressed images using our appropriate feature extraction mechanism [42]. To this intent, each of quantized AC modes pertaining to all non-overlapping $b \times b$ DCT blocks (chosen psycho-visually as $b = 8$) of an image integrates into an individual vector. For each of $(b \times b) - 1 = 63$ vectors, empirical Probability Mass Functions (PMFs) of the First Significant Digit (FSD), i.e. digits 1 to 9, and the digit 0 from the Second Significant Digit (SSD) are estimated by means of the histogram estimator [38], which result in a $(9 + 1) \times 1$ vector.

Let the function $D_L(X)$ represents the L^{th} signifcant decimal digit of the random variable $X \in \mathbb{R}$. Here, each quantized AC mode can be defined as

a random variable. Then, $D_L(X) \sim B_L$, in which B_L denotes the L^{th} digit Benford distribution. Benford's law describes the behavior of PMF as follows

$$P\left(D_L\left(X\right)=d\right)=\begin{cases}\log_{10}\left(1+\frac{1}{d}\right), & L=1 \wedge d \in \mathbb{D}_1 \\ \sum_{j=10^{L-2}}^{10^{L-1}-1}\log_{10}\left(1+\frac{1}{10j+d}\right), & L>1 \wedge d \in \mathbb{D}_0\end{cases}, \quad (1)$$

where $\mathbb{D}_0 \triangleq \{0,1,\cdots,9\}$ and $\mathbb{D}_1 \triangleq \{1,2,\cdots,9\}$. The significant decimal digit function can be explicitly obtained by [2]

$$D_L(X) \triangleq \begin{cases}0, & X=0, L>1 \\ \left\lfloor 10^{L-1}S(X)\right\rfloor - 10\left\lfloor 10^{L-2}S(X)\right\rfloor, & X\neq 0, \forall L\end{cases}, \quad (2)$$

which $S\left(X\right)$ represents the decimal significand function as

$$S\left(X\right) \triangleq \begin{cases}0, & X=0 \\ 10^{\log_{10}|X|-\lfloor\log_{10}|X|\rfloor}, & X\neq 0\end{cases}. \quad (3)$$

Note that based on the definition presented in (2), $D_1(X)$, is only counted for the non-zero real number X. But, in $D_2(X)$, both SSD of zero and non-zero numbers are considered, so that, we take into account $D_2(0) \triangleq 0$ for convenience [2]. Example 1 clearly describes determining SSD.

Example 1 (Second Significant Digit) Here, we present some examples for determining SSD as $D_2(0)=0$, $D_2(105)=0$, $D_2(0.000702)=0$, $D_2(68)=8$ and $D_2(-94)=4$.

For all AC modes, the union of PMFs determined from FSD and SSD was used as the feature vector. Therefore, the dimension of the feature space is $m = 63\times 10 = 630$, with probability values in the range $[0,\ 1]$. Because the proposed features exploit existing information into varying frequency sub-bands, they properly take into account effects of local block texture and compression's quality factor of images, which are important for forensic analysis.

To visualize information in the feature space, we reduced its dimensionality to two dimensions. The goal is to aptly identify distinctive natural clusters among the aforementioned big dataset. Hence, we have proposed a new bi-level dimensionality reduction technique consisted of a linear DR approach based on Compressive Sensing (CS) technique [8, 13] cascaded by the t-distributed Stochastic Neighbor Embedding (t-SNE) approach [28]. Then, the two-dimensional feature points are depicted in the 2-D scatterplot for further analyses.

2.1.3 Bi-level dimensionality reduction for visualization

So far, many dimensionality reduction techniques have been designed and applied to various problems of pattern recognition, such as data visualization and classification tasks [13, 16, 28, 29]. Note that the philosophy of dimensionality reduction for these tasks may be different. However, the aforementioned big image database in the emerging field of digital image forensics has two specific characteristics as follows, which seek a state-of-the-art approach to be able to visually represent information of different singly and doubly compressed databases.

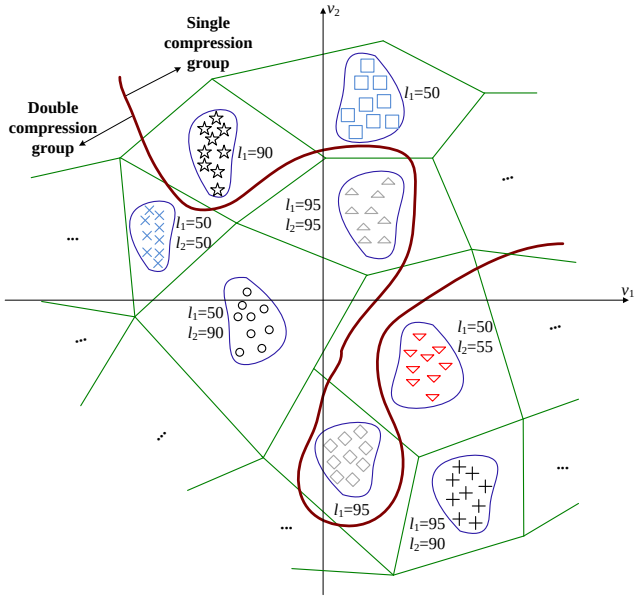

Fig. 2: Hypothesis 1 for describing the inter- and intra- category behaviors of singly and doubly compressed data points with various JPEG compression's quality levels in the two-dimensional feature space. The plot illustrates that single and double compression groups are non-linearly separable and individual classes have compact representations in the feature space partitioned by local and global decision regions.

1. Based on the first and second compression's quality levels, there are many types of singly and doubly compressed images. Therefore, we may face with hundreds of categories. For instance, in the above quality levels sampling, the number of classes, N_c, is equal to 110.
2. Different classes of single and double compression may be highly correlated and linearly non-separable in the feature space. Therefore, we will probably encounter with a non-linear feature transformation.

Hypothesis 1 (S/D compression behavior in feature space) *Let the set* $\mathcal{L} \triangleq \{\mathbf{v}_i\}_{i=1}^{N}$ *be the features of single and double compressed JPEG image patches with the first and second quality factors* $l_1, l_2 \in \mathcal{Q}$. *For computational convenience, consider* $\mathcal{Q} \triangleq \{50,\ 55,\ \ldots, 95\}$. *Then, we show in the 2-D scatterplot that the single/double compression groups are non-linearly separable and individual classes belonging to each of quality levels have compact representations (Fig. 2 illustrates that how data points of different singly and doubly compressed images lie in the feature space.).*

Proof In order to test or statistically prove Hypothesis 1 on some data, it is sufficient to visually demonstrate two issues, i.e. the distinctness of different classes and the non-linear separability of S/D compression groups. To do this, we have suggested a bi-level DR approach. At the first level, the initial feature vectors are sparsely coded based on the compressive sensing technique. The reason of this work is the fact that the amount of sparsity in blocks of Quantized DCT (QDCT) coefficients is mathematically a function of both compression's quality level and local block texture. For low compression's quality factors or textureless patches, like plain blocks and edges, QDCT coefficients are generally sparse. Consider the sparse representation of the i^{th} initial test feature vector $\mathbf{x}_i$ as the vector α_i by the following atomic decomposition

$$\mathbf{x}_i = \mathbf{\Psi}\alpha_i, \tag{4}$$

where $\mathbf{x}_i \in \mathbb{R}^m$ and $\alpha_i \in \mathbb{R}^n$. The parameters m and n are the dimension of initial features and the number of atoms, respectively. The matrix $\mathbf{\Psi} \in \mathbb{R}^{m\times n}$ denotes an over-complete dictionary. Based on the compressive sensing idea, by multiplying the measurement matrix $\mathbf{\Phi}$ by (4), we can fuse features in order to primarily diminish the initial dimensions of features as

$$\tilde{\mathbf{x}}_i = \tilde{\mathbf{\Psi}}\alpha_i, \tag{5}$$

in which $\tilde{\mathbf{x}}_i \triangleq \mathbf{\Phi}\mathbf{x}_i$ and $\tilde{\mathbf{\Psi}} \triangleq \mathbf{\Phi}\mathbf{\Psi}$. The matrix $\mathbf{\Phi} \in \mathbb{R}^{D\times m}$ is a Gaussian random matrix with the distribution $\mathcal{N}(0,\ 1)$. The parameter D denotes the number of measurements which satisfies $D < m = 630$. We set $D = 200$. Combining features speeds up the computation of a sparse estimation algorithm.

Now, the sparse vector $\alpha_i = \left[\ \alpha_1^i \ \cdots \ \alpha_n^i\ \right]$ can be estimated by solving the following optimization problem

$$\hat{\alpha}_i = \underset{\alpha_i}{\operatorname{argmin}} \left\{ \frac{1}{2} \left\| \tilde{\mathbf{\Psi}}\alpha_i - \tilde{\mathbf{x}}_i \right\|_{L_2}^2 + \lambda \|\alpha_i\|_{L_2/L_1} \right\}, \tag{6}$$

where in its second sparsitiy-inducing term, the mixed L_2/L_1-norm $\|\alpha_i\|_{L_2/L_1} \triangleq \sum_{k=1}^{N_c} \|\alpha_i^k\|_{L_2}$, for which $\alpha_i^k \triangleq \left\{\alpha_j^i \mid j \in k\right\}$. The factor $\lambda \in [0,\ 1]$ is a regularization parameter that we set $\lambda = 0.5$. Eq. (6) is defined as the group Least Absolute Shrinkage and Selection Operator (LASSO) [6, 23].

At the second level, for visualizing, the dimensions of sparse feature vectors are reduced to $\nu < n$, by the non-linear t-SNE algorithm. This approach is an unsupervised and non-parametric DR technique. The idea behind t-SNE algorithm is to construct two probability distributions stemmed from pairwise similarities among data points in both high- and low- dimensional spaces. Taking into account local structures of data points in the low-dimensional space, the algorithm iteratively minimizes an objective function based on the Kullback-Leibler divergence between two distributions. The proposed bi-level DR technique is summarized in Algorithm 1.

For visualizing the low-dimensional features $\mathbf{v}_i,\ \forall i$, we set the reduced dimensions as $\nu = 2$ which donates a good and certain visual perception to

Algorithm 1 The proposed bi-level visualizer algorithm

1: **Input**: Patterns, i.e. the initial features and their labels.
2: Determine the number of atoms as $n = N_c \times T_{ls}$, where T_{ls} is the number of learning-set images for each class.
3: Choose randomly n samples with replacement as the dictionary so that $\mathbf{\Psi} = \{ \mathbf{\Psi}_1 \ \mathbf{\Psi}_2 \ \cdots \ \mathbf{\Psi}_{N_c} \}$, where the matrix $\mathbf{\Psi}_j$, $\forall j \in [1, N_c]$, includes samples of the j^{th} class.
4: Determine the total number of samples for testing as $N = N_c \times T_{ts}$, where T_{ts} represents the number of testing-set images for each class.
5: Choose randomly N samples with replacement as the testing-set. Please note that random learning and testing samples from each class are equal.
6: Generate the measurement matrix $\mathbf{\Phi}$.
7: Calculate $\tilde{\mathbf{\Psi}} = \mathbf{\Phi}\mathbf{\Psi}$.
8: **for** $i \leftarrow 1, N$ **do**
9: Calculate $\tilde{\mathbf{x}}_i = \mathbf{\Phi}\mathbf{x}_i$.
10: Determine $\hat{\alpha}_i$ as (6) by solving the group LASSO.
11: Set $\mathcal{D}\{i\} \leftarrow \hat{\alpha}_i$.
12: **end for**
13: Map the matrix $\mathcal{D}$ onto the low-dimensional representation matrix $\mathcal{L}$, by t-SNE DR algorithm.
14: **Output**: The dimensionally reduced features $\mathcal{L}$.

the analyst in the 2-D orthogonal coordinate system. Therefore, to represent point clouds $\mathbf{v}_i = \left[v_1^i \ v_2^i \right]^{\mathrm{T}}$, $\forall i$, in the feature space, we employ the 2-D scatterplot. For each S/D compressed type, a unique color/symbol code is utilized. In Fig. 3, the 2-D scatterplot of different color- and/or symbol- coded types of single and double compressed JPEG image patches are drawn which verifies Hypothesis 1. In order to create singly and doubly compressed image patches for testing Hypothesis 1, McGill Calibrated Colour Image Database (CCID) raw image-sets has been utilized [32]. Fig. 4 shows the color/symbol codes of different types used in the scatterplot. Note that for all point clouds, the ground truth label is only used to select a color/symbol code for visual encoding of a data point.

The visualization results demonstrate that clusters pertaining to double compressed classes are well separated and matched to natural sub-groups, except the single compressed types having the compression's quality level l_1 with those of double compressed ones having $l_2 = l_1$ as well as a central elliptical region in which 16 individual types are mixed together. The exceptional cases are generally related to the nature of the proposed features, especially in the situation $l_1 = l_2$. The central entangled data points include the classes C_5, C_6, C_7, C_{45}, C_{55}, C_{56}, C_{61}, C_{65}, C_{66}, C_{73}, C_{77}, C_{78}, C_{93}, C_{97}, C_{103} and C_{105}. □

2.2 Bottom-up quantization estimation and DJCD

Starting from intuitions of the visualization described in Section 2.1, we have established the proposed bottom-up learning strategy for estimating quality level and detecting double compression as follows.

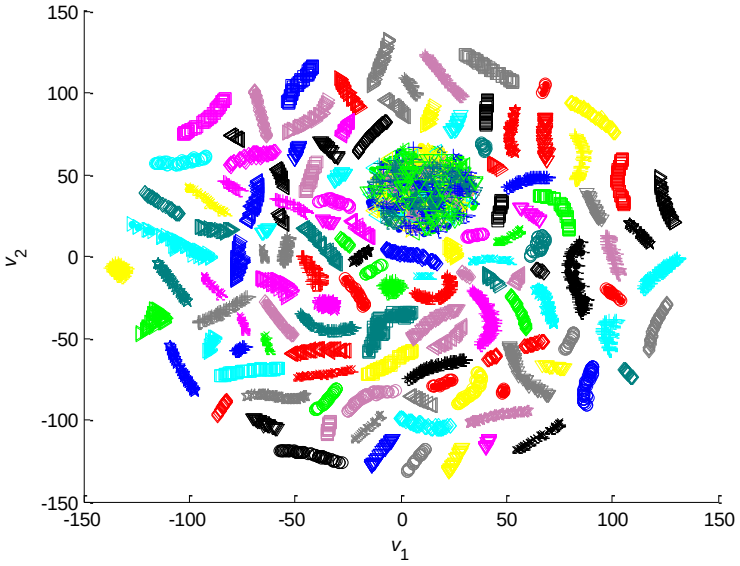

Fig. 3: The visualization results of the proposed dimensionality reduction technique which satisfy Hypothesis 1. The point clouds are pertaining to 110 color- and/or symbol- coded types of 27500 singly and doubly compressed JPEG images created by original raw McGill Calibrated Colour Image Database (CCID) image-set [32]. To avoid the overdraw problem, we only depicted 6600 point clouds so that, for each class, 60 samples were randomly chosen for showing.

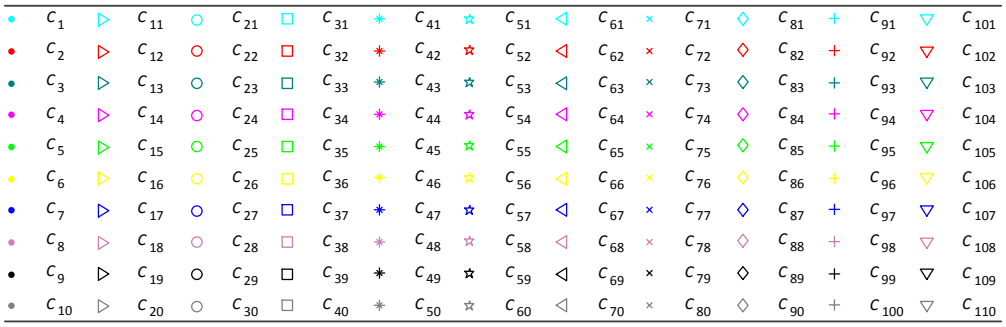

Fig. 4: The color/symbol codes of different classes used in all scatterplots of this paper.

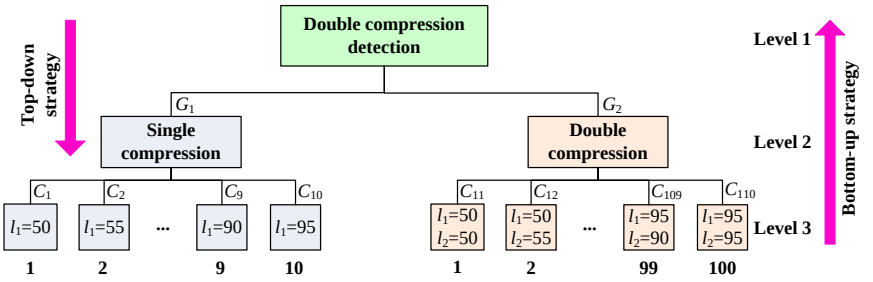

Fig. 5: The hierarchy of the proposed bottom-up and top-down learning strategies for identifying the traces of double JPEG compression. Top-down learning strategy breaks the problem of double compression detection down into two levels, whereas bottom-up style is a three-level process.

1. The feature space shown in Fig. 3 reveals important information, for which different types of singly and doubly compressed JPEG images are distinctive and can be accurately clustered. Accordingly, we propose a BU learning system for DJCD (BU-DJCD) which takes each sub-database of the big database into account as an individual class.
2. To design the BU detector, various generative or discriminative models [44] can be employed for matching/learning distinctive natural clusters. Here, we utilized a discriminative linear Support Vector Machines (SVMs) classifier [5] to construct the mentioned multi-class classification system.

The hierarchy of the bottom-up learning strategy for detecting double JPEG compression is drawn in Fig. 5. As it is obvious in this figure, because of the estimation from low-level to high-level in the BU style, this can preserve locality among varying types of single and double compressed data. In other words, sub-categories collaborate to make a high-level decision. In Fig. 6, the block diagram of the proposed BU learner, enclosed with a blue dotted rectangle, is depicted. In the following sub-sections, we independently describe the proposed BU style in quantization- unaware and semi-aware scenarios.

2.2.1 Quantization-unaware BU-DJCD

Based on the quality level sampling of l_1 and $(l_1,\ l_2)$ respectively for the first and second compression in Definition 1, there are 110 classes in the quantization-unaware scenario to design the related multi-class classification system based on a one-versus-one division mechanism. In this case, one learned model is obtained to estimate the quality level as well as detect double compression for a query test image. Once the unknown quality factors l_1 and/or $(l_1,\ l_2)$ have been estimated, the corresponding quantization tables, concerned with the baseline JPEG quantizer, can be uniquely identifiable. By a two-category grouping of real clusters from the level 3 of Fig. 5 into summary

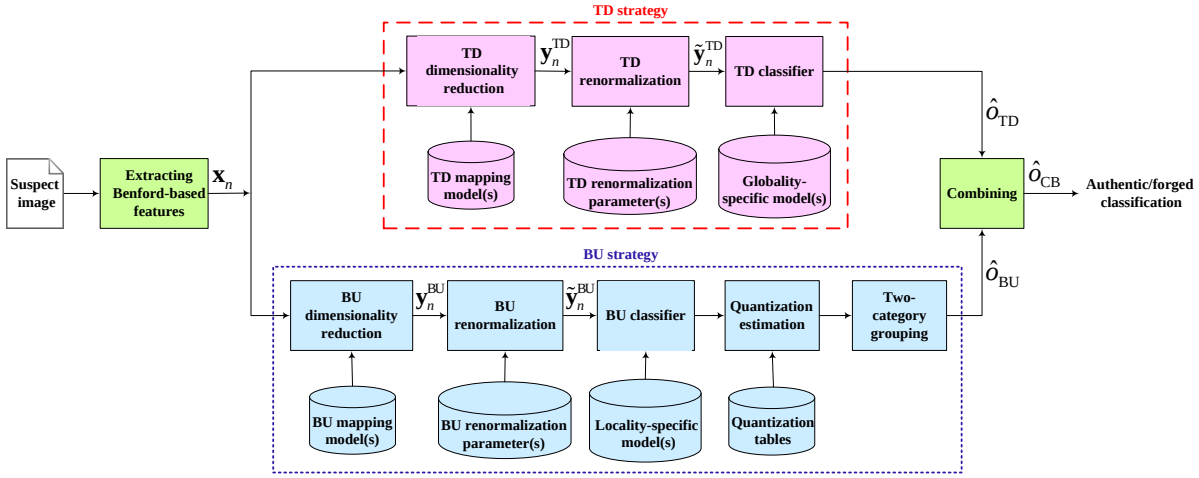

Fig. 6: The block diagram of the proposed perceptual Top-Down/Bottom-Up (TD/BU) detector composed of two complement TD and BU learner systems. TD and BU strategies are enclosed with red dashed and blue dotted rectangles, respectively.

groups of its level 2, we can classify the test image into singly or doubly compressed group.

2.2.2 Quantization-semi-aware BU-DJCD

In the quantization-semi-aware scenario, because the last compression history is known, the number of classes reduces to 11, one class for single compression and other 10 classes representing double compression types. For instance, let $l_1 = 75$ or $l_2 = 75$, in which the database corresponding to the first quality level $l_1 = 75$ construct one-class pertaining to single compression group and the combinations $\{(50,\ 75),\ (55,\ 75),\ \ldots,\ (95,\ 75)\}$ encompass 10-class pertaining to double compression group (Please see Table 1.). Ultimately, for each known last compression quality level, we determine an individual learned model by the one-versus-one strategy, i.e. $|\mathcal{Q}| = 10$ classification models are stored to use in the testing phase for discriminating singly compressed images from doubly compressed ones as well as estimating its primary quantizer.

2.3 Top-down DJCD

As mentioned before, the proposed BU methodology takes into account locality among different clusters. However, it is not sufficient to grasp a robust double compression detector and a holistic insight into groups is also required. In this

regard, general information about the population of single and double compressed images make a good sense to coarsely discriminate their areas. This goal can be attainable by considering a rough classifier called top-down learner system (TD-DJCD) to discover the global structure of singly and doubly compressed data. In the TD-DJCD, the image under analysis is coarsely classified into two groups, i.e. single and double compression, without knowledge about the behavior of compressed images having different quality levels. Fig. 5 shows the hierarchy of the proposed top-down learning strategy for detecting double JPEG compression. The block diagram of the TD strategy, enclosed with a red dashed rectangle, is depicted in Fig. 6.

For the TD strategy in the quantization-unaware scenario, 110 types of single and double compression groups are firstly divided into two groups. Then, we feed feature vectors of all training images to a binary SVMs classifier to obtain a single globality-specific model. About the quantization-semi-aware case, for each known last compression history, 11 types described in Section 2.2.2, are categorized into two groups, so that we have one class for single compression group and others for double compression. Again, we employ a binary SVMs learner to determine the relevant models. Totally, $|\mathcal{Q}| = 10$ learned models from the TD learner are exploited in the quantization-semi-aware scenario.

2.4 PCA dimensionality reduction for classification

Although our initial features appropriately exploit existing information into the total space of AC modes, to train a detector, it may be required to reduce the dimension of original features for preventing the probable curse of dimensionality, especially in small data (e.g. for forgery localization purposes). For such a classification task, the suggested bi-level DR technique dedicated to the visualization purpose cannot be efficiently utilized. It is due to the fact that the t-SNE dimension reduction approach, employed at the second level of our DR method, does not deliver an explicit mapping for the feature space. In order to overcome this problem for reducing the dimension of a query test data, a solution is to combine that one with the whole dataset and recalculate the DR process again. However, because of inefficiency in the computation, this way does not recommend. Instead, different parametric dimensionality reduction techniques can be utilized for classification [29]. Here, we used the data-driven Principal Component Analysis (PCA) dimension reduction technique [15, 33]. We will empirically demonstrate in Section 3 that PCA compensates and yet preserves an appropriate discrimination power between S/D compression species like the proposed visualizer by, of course, the optimum feature dimensions much more than $\nu = 2$ [27]. Factually, PCA is a variant of the optimal Karhunen-Loève Transform (KLT) that aptly encodes information of different quantized frequency sub-bands into a lower-dimensional representation.

For both TD and BU strategies whether in quantization- unaware or semi-aware scenario, the mapping models of the unsupervised PCA dimensionality

Algorithm 2 The learning process of the proposed double JPEG compression detection algorithm

1: **Input**: Learning images set of a given database.
2: Dump QDCT coefficients of an image.
3: Integrate each quantized AC mode belonging to all blocks of an image into an individual vector.
4: Estimate PMF of the FSD (i.e. digits 1 to 9) for each vector.
5: Estimate PMF of the digit 0 from the SSD for each vector.
6: Create feature vector by unifying distributions obtained from Steps 4 and 5.
7: Apply PCA for the low-dimensional model and then, renormalize the dimensionally reduced features.
8: Feed feature vectors of all training images to a SVMs classifier to determine the learned model.
9: **Output**: The PCA mapping model, the renormalization parameters and the learned model.

reduction technique are calculated from learning instances without their labels. After dimensionality reduction, for each strategy, a renormalization step is applied to the reduced features. The renormalization parameters are $\mu^{\mathcal{S}}$ and $\sigma^{\mathcal{S}}$, denoting the sample mean and standard deviation vectors, respectively, in which $\mathcal{S} \triangleq \{\text{TD, BU}\}$. These parameters determined by all learning low-dimensional ensembles. The renormalization for the n^{th} training/testing low-dimensional sample, $\mathbf{y}_n$, in the range $[0,\ 1]$ is done as

$$\tilde{\mathbf{y}}_n^{\mathcal{S}} = \left(\mathbf{y}_n^{\mathcal{S}} - \mu^{\mathcal{S}}\right) \circledcirc \sigma^{\mathcal{S}},\ \forall \mathcal{S}, \tag{7}$$

in which the notation $\circledcirc$ stands for the entry-by-entry right division and $\mathbf{y}_n^{\mathcal{S}} = \left(\mathbf{T}^{\mathcal{S}}\right)^{\mathrm{T}} \mathbf{x}_n,\ \forall \mathcal{S}$. The vectors $\mathbf{x}_n$ and $\tilde{\mathbf{y}}_n^{\mathcal{S}},\ \forall \mathcal{S}$, represent the Benford-based and renormalized features from the n^{th} sample, respectively. For the TD and BU strategies, the PCA transformation kernels of a given model are $\mathbf{T}^{\mathrm{TD}} \in \mathbb{R}^{m \times d_r^{\mathrm{TD}}}$ and $\mathbf{T}^{\mathrm{BU}} \in \mathbb{R}^{m \times d_r^{\mathrm{BU}}}$, respectively. Because the TD learner is rich in training instances, we allow to set $d_r^{\mathrm{TD}} \geqslant d_r^{\mathrm{BU}}$. Typically, we can summarize the learning phase of the proposed DJCD algorithm in Algorithm 2.

2.5 Combined top-down/bottom-up DJCD approach

The original inspiration of our idea connects to the areas of study in cognitive science. Here, we describe the idea behind the proposed perceptualized mechanism for detecting double compression as the following geographical locations labeling. Let the problem be to segment zones of the earth. As a solution, suppose a person observes the globe from a distant point, e.g. in space. Observer may globally categorize the earth into two groups, namely land and ocean. We call this process as a TD approach which segments areas fast, but do not attend to details. Now, consider another way in which a person traverses on the earth. During travel, observer is encountered with various areas, like city, forest, desert, mountain, river, lake, sea, etc. In accordance with this labeling scheme, a different categorization from TD process may be introduced. We

call this procedure as a BU approach which takes into account local structures accurately, but has not a general perception of zones situation. Therefore, a mixed version of two schemes seems to be the best labeling.

In our problem, the proposed TD algorithm takes into account global knowledge to gain surrounding types of an individual group. And, BU approach considers locality. On the other hand, our empirical assessments also confirm that TD strategy discriminates single compressed images better than double compressed ones, whereas BU processing operates just inversely. Therefore, TD and BU learning strategies are complementary to each other in nature. Based on this complementarity fact, we constructed a combined strategy to synergistically alleviate the drawbacks of TD and BU learning strategies and reinforce their strengths. Fig. 6 depicts the block diagram of the proposed combined perceptual TD/BU approach in the testing phase. The combined scheme in quantization-unaware case has two learned models, one for TD strategy and another for BU method. For the quantization-semi-aware scenario, they are 20 models with an equal portion of each learner.

In the proposed method, the prediction results of both TD and BU double compression detectors, $\hat{o}_{\mathcal{S}}$, $\forall \mathcal{S}$, are binarized with the relevant real-valued confidence levels, i.e. $P^{\mathcal{S}} \in [0,\ 1]$, $\forall \mathcal{S}$. Factually, the mentioned confidence levels represent posterior class probabilities that are obtained by the algorithm suggested in [20]. We generate a truth table for combining TD and BU results to finally make a mid-level decision, i.e. the output $\hat{o}_{\mathrm{CB}}$. Hence, there are four possible cases for the outputs of $\hat{o}_{\mathrm{TD}}$ and $\hat{o}_{\mathrm{BU}}$. If the results of $\hat{o}_{\mathrm{TD}}$ and $\hat{o}_{\mathrm{BU}}$ are the same, whether single or double compression, then the combiner will confirm them; else, if the predictions of TD and BU systems are different, then the final prediction of the combination is that one with more confidence level as

$$\hat{o}_{\mathrm{CB}} = \underset{i}{\operatorname{argmax}}\, \mathbf{c}\ , \tag{8}$$

in which the vector $\mathbf{c}$ includes the confidence levels of TD and BU classifiers, i.e. $\mathbf{c} = \left[\, P^{\mathrm{TD}}\ P^{\mathrm{BU}} \,\right]^{\mathrm{T}}$.

2.6 Image forgery detector

The proposed BU, TD and combined TD/BU approaches can be also employed in locating tampered regions of manipulated JPEG images by using a sliding-window forgery detector. For this purpose, in the compressed domain, we first scan the whole non-overlapping $b \times b$ blocks of the questionable JPEG image $\mathbf{I}$, with the width of w and height of h, by using a sliding square mask with the length of $\omega = 2z + 1$ blocks, in which $z \in \mathbb{N}_0$ (The symbol $\mathbb{N}_0$ denotes the set of all nonnegative integer numbers.). We set $z = 2$. Then, for each mask, the operations depicted in Fig. 6 are performed. If the decision is double compression, we set the pixels corresponding to the central block 0 in the resulting binary image $\mathbf{B}$. Otherwise, they are set 1. To scan the

whole non-overlapping blocks of the image $\mathbf{I}$, the aforementioned operations are repeated N_b times, where $N_b = \left\lceil \frac{w}{b} \right\rceil \times \left\lceil \frac{h}{b} \right\rceil$ is the total number of image blocks for which $\lceil \cdot \rceil$ denotes the ceiling function.

Ultimately, a tri-step post-processing stage is applied to the binary image $\mathbf{B}$ in order to respectively connect breaks by the morphological dilation operator with the square structure element of the length of 19, remove noisy segments (i.e. connected component objects that have areas less than the predefined threshold $t = 0.03\,(w \times h)$), and fill holes via a morphological reconstruction algorithm proposed in [39]. Specifically, Algorithm 3 describes the pseudo-code of the proposed combined TD/BU image forgery detector algorithm, which is able to locate altered regions in real image forgery detection applications. And, as shown in Fig. 6, this algorithm is similarly simplified for the proposed TD and BU learning strategies.

3 Experiments and evaluations

In this section, we first compare the separation capability of the suggested visualizer with the modern methods published in [1, 13, 28]. Afterwards, taking into account both quantization- unaware and semi-aware scenarios, the performance of our approaches for detecting double JPEG compression and estimating the first quality level are assessed. Then, the proposed forgery locating algorithm will be examined in a real image forgery scenario. We compare the performance of these forensic techniques with the state-of-the-art related approaches of [3, 7, 18, 19, 31]. We also exploited standard performance metrics to empirically appraise the robustness and generalization capabilities of different methods which will be described in the tests.

Algorithm 3 The pseudo-code of the proposed combined TD/BU image forgery detector algorithm

Input: The questionable image $\mathbf{I}$ in JPEG format.
Read coder information and then, dump the QDCT coefficients matrix, $\mathbf{Q}$, of the image $\mathbf{I}$.
for $i \leftarrow 1, N_b$ **do**
    Put the center of the mask of $\omega \times \omega$ blocks on the i^{th} block of the matrix $\mathbf{Q}$.
    Extract features.
    Feed concurrently the feature vector to TD and BU classifiers with the related coder quality level.
    Combine results of $\hat{o}_{\mathrm{TD}}$ and $\hat{o}_{\mathrm{BU}}$ to make $\hat{o}_{\mathrm{CB}}$.
    if $\hat{o}_{\mathrm{CB}}$ is double compression **then**
        Set $\mathbf{B}\{i\} \leftarrow \mathbf{O}$, where $\mathbf{O}$ represents a $b \times b$ zero matrix.
    else
        Set $\mathbf{B}\{i\} \leftarrow \mathbf{J}$, where $\mathbf{J}$ represents a $b \times b$ all-ones matrix.
    end if
end for
Apply the tri-step post-processing stage to the binary image $\mathbf{B}$ in order to create the ultimate segmented image $\mathbf{F}$.
Output: The segmented image $\mathbf{F}$.

In experiments and evaluations, three real-world databases of raw images were utilized to learn and assess the proposed approaches against various databases with different statistics of size, textural information and image dimensions as follows.

- McGill CCID: This database consists of raw images with Tagged Image File Format (TIFF) extension [32]. It encompasses a wide range of textured color images from animals, flowers, foliage, fruits, landscapes, man-made, shadows, winter and textures categories, taken with two Nikon Coolpix 5700 digital cameras from natural scenes of dimensions 768×576 or 576×768. In these 9 categories, 56 samples of all 1152 raw images were the same. Hence, in all experiments of this paper, we removed these repeated images to attain 1096 raw images.
- Never-compressed Color Image Database (NCID): This database contains 5150 raw BMP image patches of dimensions 256×256 [24, 25].
- Raw Color Image Database (RCID): This database encompasses 208 raw images that authors have captured by a Canon Eos 550D digital color camera from natural scenes with TIFF extension and full capacity of resolution, i.e. dimensions 5184×3456 or vice versa[2].

From the textural contents viewpoint, the RCID, CCID and NCID image-sets generally contain low-, moderate- and high- textured images, respectively.

3.1 Separation capability of visualizer

In this experiment, we used McGill CCID database to create singly and doubly compressed JPEG images. We depicted in Section 2.1.3 the separation capability of the proposed visualizer to show that classes of singly and doubly compressed JPEG images with different compression's quality levels coincides with natural clusters. In the proposed visualizer, the number of learning- and testing- set images for each class were set equally, so that $T_{ls} = T_{ts} = 250$ chosen randomly from databases. Therefore, $110 \times 250 = 27500$ images were used for testing our information visualizer.

We also compared the suggested visualization algorithm with the supervised kernel Fisher Linear Discriminant (FLD) [1], semi-supervised CS-PCA-L_2/L_1 [13] and unsupervised t-SNE [28] DR approaches. Similar to the proposed visualizer, we employed the 2-D scatterplot in order to observe the segregation capability of different information visualization techniques. For a fair comparison, the experimental setup of the competing approaches was exactly identical with our visualizer, too. The utilized kernel in the kernel FLD method was a Gaussian Radial Basis Function (RBF) with the variance 1.

Figs. 7 (a), (b) and (c) portray the separation quality of the kernel FLD, CS-PCA-L_2/L_1 and t-SNE algorithms in the 2-D scatterplots, respectively. For

[2] The RCID database is publicly available to fellow academic researchers. For accessing this database, please contact behrad@shahed.ac.ir.

showing and avoiding the overdraw problem, we only depicted $110 \times 60 = 6600$ point clouds, i.e. for each class, 60 samples were randomly chosen. Contrary to the proposed visualizer, other's results reveal that data points from various classes are either entangled, especially in the method [1], or overlapped with each other. In the algorithm [13], the grouped point clouds are mostly mapped onto the origin. Among the competing approaches, only the non-linear t-SNE algorithm separates better natural classes in the 2-D feature space. Therefore, the proposed algorithm achieves a good separation of natural clusters compared to the state-of-the-art techniques for the reduced dimension of $\nu = 2$.

3.2 Detection efficiency of double compression

3.2.1 Performance with quantization-unaware scenario

In this experiment, we employ the benchmark raw images database of CCID to create singly and doubly compressed JPEG images for training/testing classification systems. Based on the holdout cross-validation approach, 75% of each sub-database is employed to learn TD and BU classifiers and the remainder data are made the test-set. Total samples of the single compression group were $10 \times 1096 = 10960$ images, whereas they were $100 \times 1096 = 109600$ images for the double compression group. This fact denotes a skewed class distribution with between-group imbalance ratio 10:1 for TD double compression detector. To provide a balanced distribution in the learning phase of TD classifier, we used the oversampling method [14] wherein the data of the single compressed group were replicated 10 times for SVMs adjusted to the same weights of groups and the unit cost. Therefore, learning instances for TD and BU classifiers were altogether $(10 \times 10 + 100) \times 0.75 \times 1096 = 164400$ and $110 \times 0.75 \times 1096 = 90420$, respectively. And, all testing instances for these classifiers were $110 \times 0.25 \times 1096 = 30140$ images.

We also compared the performance of the proposed TD, BU and combined TD/BU approaches with that of methods B. Li et al. [18], Milani et al. [31], and Dong et al. [7]. Table 2 presents the confusion matrix of different methods for the 2-group classification problem in the quantization-unaware scenario. The table's entries comprise the conditional probabilities of $P(G_2|G_2)$, $P(G_1|G_2)$, $P(G_2|G_1)$ and $P(G_1|G_1)$ in percentage, which represent True Positive (TP), False Negative (FN), False Positive (FP) and True Negative (TN), respectively. As it can be seen, the proposed BU strategy indicates the best TP among competitors. But, due to high FP, it is not reliable to authenticate a previously original single compressed image in the quantization-unaware scenario. Relatively speaking, the suggested TD scheme and methods [7, 18, 31] provide reverse behaviors which is not desirable from a forensic analyzer viewpoint. Generally, the misclassifying cost of the group G_2 as G_1 is more expensive than the group G_1 as G_2; because a predicted doubly compressed image may be examined in further forensic tools for locating its probable tampered regions, whereas an identified singly compressed image is generally known as

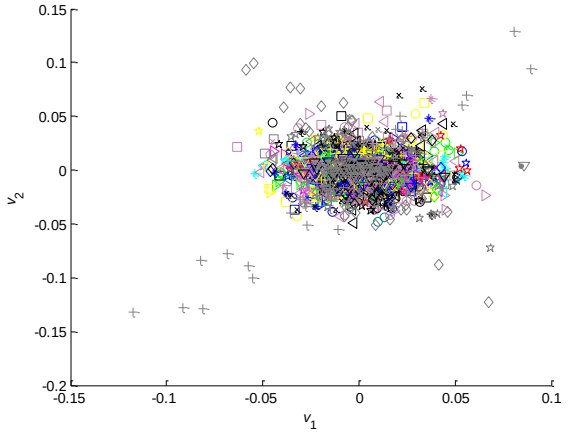

(a)

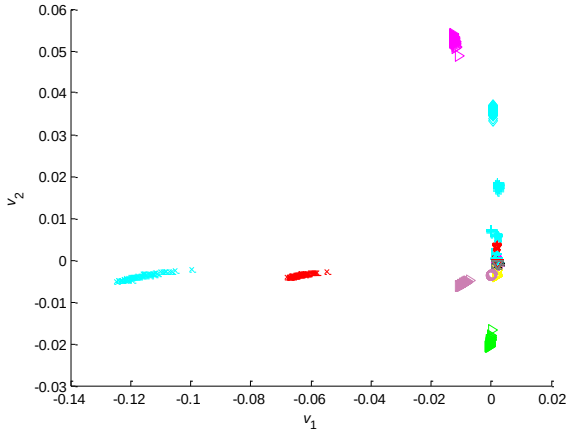

(b)

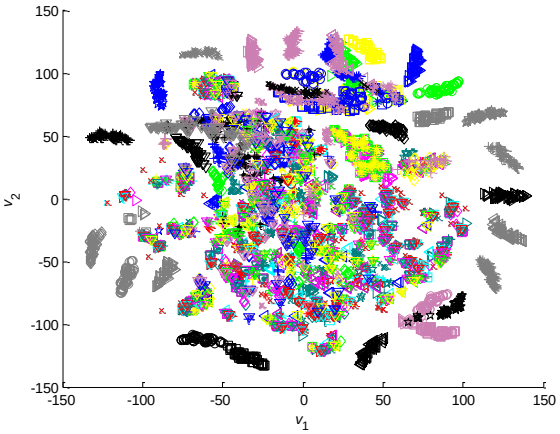

(c)

Fig. 7: The visualization results of 27500 singly and doubly compressed JPEG images by the competing (a) kernel FLD [1], (b) CS-PCA-L_2/L_1 [13] and (c) t-SNE methods [28]. To avoid the overdraw problem, we only depicted 6600 point clouds so that, for each class, 60 samples were randomly chosen for showing.

Table 2: Confusion matrix for the 2-group classification problem in different approaches on original raw McGill CCID image-set in terms of percentage

Confusion matrix		Ground truth											
		G_2						G_1					
		Method [18]	Method [31]	Method [7]	TD strategy	BU strategy	Fused TD/BU	Method [18]	Method [31]	Method [7]	TD strategy	BU strategy	Fused TD/BU
Predicted result	G_2	51.21	33.00	52.09	58.59	94.18	88.02	3.54	9.09	4.38	5.77	48.69	16.9
	G_1	48.79	67.00	47.91	41.41	5.82	11.98	96.46	90.91	95.62	94.23	51.31	83.1

an authentic content. Nevertheless, the proposed combined TD/BU approach represents reasonable TP and TN with tolerable FN and FP which make it ideal for quantization-unaware double compression detection.

In order to interpret the effectiveness of different methods more deeply, some standard performance metrics were assessed from the confusion matrix tabulated in Table 2. These metrics consist of

$$\text{Sensitivity}=\frac{\text{TP}}{\text{TP}+\text{FN}}, \tag{9}$$

$$\text{Specificity}=\frac{\text{TN}}{\text{TN}+\text{FP}}, \tag{10}$$

$$\text{Accuracy}=\frac{\text{TP}+\text{TN}}{\text{TP}+\text{FN}+\text{FP}+\text{TN}}, \tag{11}$$

$$G\text{-mean} = \sqrt{\text{Sensitivity} \times \text{Specificity}}, \text{and} \tag{12}$$

$$F_1\text{-measure} = \frac{2\text{TP}}{2\text{TP}+\text{FP}+\text{FN}}. \tag{13}$$

In the quantization-unaware scenario, the performance metrics of different methods on CCID database are summarized in Table 3 in terms of percentage. In addition to total Sensitivity which represent the performance on double compression classification, we separately figured out this forensically important criterion for compression's quality level settings of $l_1 < l_2$, $l_1 = l_2$ and $l_1 > l_2$, to investigate the robustness of various double compression detection techniques against different compression's quality factors. In Table 3, the highlighted values in the bold type represent the best performance. The metrics demonstrate that the results of the proposed BU strategy are promising especially in double compression detection. Its F_1-measure score improvement to the best competing approach [7] is equal to 26.32%. However, based on the Geometric-mean (G-mean) criterion, the proposed combined TD/BU approach is able to balance the performance between the minority group, i.e. single compression, and the majority group, i.e. double compression, more efficiently, as is desired in practice.

Table 3: Performance metrics of different approaches on original raw CCID database for the quantization-unaware double JPEG compression detection in percentage

Method	Performance metrics							
	Sensitivity				Specificity	Accuracy	G-mean	F_1-measure
	$l_1 < l_2$	$l_1 = l_2$	$l_1 > l_2$	Total				
B. Li et al. method [18]	84.96	3.58	28.05	51.21	**96.46**	55.33	70.28	67.58
Milani et al. method [31]	51.56	8.98	19.79	33.00	90.91	38.27	54.78	49.29
Dong et al. method [7]	85.39	4.38	29.40	52.09	95.62	56.05	70.58	68.31
Proposed TD strategy	84.91	5.73	44.03	58.59	94.23	61.83	74.31	73.62
Proposed BU strategy	**99.8**	**47.15**	**99.02**	**94.18**	51.31	**90.29**	69.52	**94.63**
Proposed combined TD/BU approach	98.54	16.64	93.37	88.02	83.1	87.57	**85.53**	92.8

For all l_1 and l_2 in the set $\mathcal{Q}$, Tables 4, 5, 6, 7, 8 and 9 tabulate the detailed detection accuracies of [7, 18, 31], and the proposed TD, BU and the combined TD/BU methods, respectively. In these tables, A_{G_1} and A_{G_2} denote detection accuracies for G_1 and G_2 groups in terms of percentage, respectively. To make sense of the assessment, among the compared methods listed in Tables 4, 5, 6, 7, 8 and 9, the highlighted values in the bold type indicate the best performance for each l_1 and $(l_1,\ l_2)$ in single and double compression groups, respectively. Obviously, the results prove the robustness of the proposed perceptual method against different compression's quality level settings.

For further comparative analysis of the robustness and stability in different approaches, we compare here the proposed perceptual TD/BU approach to our TD method, which this strategy alone is even more effective than the competing methods [7, 18, 31]. For instance, Fig. 8 (a) portrays the accuracy curves of the proposed TD learning strategy in order to detect double compression, A_{G_2}, in terms of l_2 for $l_1 = 50,\ 95$. As shown in this figure, the instability behavior in double compression detection is clear when $l_1 > l_2$. Fig. 8 (b) depicts exactly these accuracy curves for the proposed combined TD/BU approach. In comparison to Fig. 8 (a), it indicates the stability in double JPEG compression detection for the challenging case $l_1 > l_2$.

In all experiments of this paper, the reduced feature dimensions for TD and BU learning strategies were determined in such a way that they maximize the G-mean criterion. Hence, for optimizing the parameters d_r^{TD} and d_r^{BU}, we experimentally changed their range from 10 to 300. In current experiment, for the quantization-unaware BU-DJCD, we utilized $d_r^{\mathrm{BU}} = 150$, as an optimum value. Here, due to the availability of huge observation data for training the TD classifier, we did not apply the PCA dimensionality reduction for the TD learning strategy.

Table 4: The detection accuracies of B. Li et al. method [18] on original raw CCID database. A_{G_1} and A_{G_2} denote detection accuracies for G_1 and G_2 groups in terms of percentage, respectively.

A_{G_2}		l_1									
		50	55	60	65	70	75	80	85	90	95
l_2	50	8.03	7.66	1.82	23.72	6.2	98.18	96.35	20.8	16.06	6.93
	55	23.36	6.2	29.2	0.73	0	0	3.65	0.73	69.71	5.84
	60	41.61	12.41	6.2	79.56	41.97	6.93	86.13	59.49	7.66	15.69
	65	85.04	8.39	35.4	8.39	81.02	0.73	0.73	40.88	4.38	2.55
	70	92.34	93.43	94.89	15.33	4.74	29.93	0	98.18	70.8	4.38
	75	99.27	99.27	97.81	99.64	19.71	1.46	87.59	0	20.07	1.46
	80	99.27	95.62	96.72	97.45	98.91	74.82	0.36	77.01	0	1.46
	85	98.54	99.64	99.64	98.91	98.54	94.16	91.97	0	51.09	4.74
	90	96.72	98.18	99.64	97.81	97.45	96.72	98.18	97.45	0	0
	95	96.35	98.91	100	97.08	100	97.08	94.53	95.62	99.64	0.36
A_{G_1}		91.97	93.8	**93.8**	91.97	**94.89**	98.54	99.64	**100**	**100**	**100**

Table 5: The detection accuracies of Milani et al. method [31] on original raw CCID database in terms of percentage

A_{G_2}		l_1									
		50	55	60	65	70	75	80	85	90	95
l_2	50	16.06	8.39	7.3	22.63	84.67	9.12	83.94	17.52	21.17	16.42
	55	21.17	16.42	11.31	3.28	16.42	12.41	4.01	5.47	17.88	16.06
	60	8.39	36.13	12.04	21.17	17.15	39.05	20.8	48.91	8.76	12.04
	65	83.21	4.38	43.43	10.95	19.71	3.28	17.88	9.49	8.76	10.58
	70	3.65	77.37	46.35	4.74	9.49	51.82	1.09	20.8	12.41	9.12
	75	3.28	29.93	47.45	61.68	3.28	8.76	95.99	2.92	14.96	9.12
	80	95.99	78.1	59.85	21.17	55.84	0.73	5.84	43.07	7.3	6.57
	85	96.72	99.64	98.91	36.5	0.36	17.88	21.9	4.38	5.47	2.55
	90	24.45	82.48	75.91	97.81	4.38	98.91	4.01	99.64	5.11	11.68
	95	13.14	87.23	82.85	62.04	85.04	88.32	72.99	99.64	83.21	0.73
A_{G_1}		83.58	83.58	87.96	89.05	90.51	91.24	94.16	95.26	94.89	98.91

3.2.2 Performance with quantization-semi-aware scenario

Similar to the above quantization-unaware tests, we utilize McGill CCID database to train/test different methods in the quantization-semi-aware scenario. In this experiment, 75% of each sub-database is employed to learn the classifiers. The remainder data are contained the test-set. For the quantization-

Table 6: The detection accuracies of Dong et al. method [7] on original raw CCID database in terms of percentage

A_{G_2}		l_1									
		50	55	60	65	70	75	80	85	90	95
l_2	50	12.04	11.31	2.55	30.29	16.06	98.18	96.35	18.61	26.64	9.49
	55	27.01	9.49	30.29	0	0.73	0	6.93	2.19	58.03	10.58
	60	50.73	16.06	7.66	75.18	44.89	10.22	83.58	58.39	11.68	20.07
	65	82.85	10.22	39.78	8.03	82.48	0	0	48.54	1.46	2.55
	70	85.4	92.34	93.8	24.09	5.47	35.4	0	97.45	79.56	5.84
	75	98.91	98.91	95.26	98.91	15.69	1.09	84.31	0.73	21.17	0.73
	80	99.27	95.62	95.99	96.72	99.64	77.37	0	79.2	0	2.55
	85	98.18	99.64	99.64	98.91	98.18	94.16	95.26	0	50.73	8.03
	90	97.08	98.91	100	97.81	99.27	97.45	97.81	98.18	0	0
	95	98.18	98.18	100	97.08	99.64	96.35	94.53	94.89	98.91	0
A_{G_1}		87.96	90.51	92.34	91.97	94.53	**98.91**	**100**	100	100	100

Table 7: The detection accuracies of the proposed TD learning strategy on original raw CCID database in terms of percentage

A_{G_2}		l_1									
		50	55	60	65	70	75	80	85	90	95
l_2	50	6.93	8.76	1.82	39.78	20.07	89.42	93.07	31.02	26.64	22.99
	55	28.1	5.47	31.02	5.11	2.19	0	2.19	2.55	82.48	2.55
	60	60.22	8.39	7.66	35.4	54.74	16.42	93.07	58.03	41.24	62.41
	65	80.66	32.48	41.97	7.66	88.69	28.83	19.71	38.69	13.87	1.82
	70	81.39	85.4	80.66	50.36	11.68	62.41	21.9	97.81	75.91	64.96
	75	95.99	98.91	92.7	97.81	27.01	4.38	89.42	1.46	85.04	17.52
	80	98.18	93.8	92.34	88.32	98.91	73.36	2.55	79.93	59.49	67.15
	85	97.45	97.08	98.18	94.16	97.45	94.16	95.26	1.82	75.18	86.13
	90	93.8	96.72	98.54	96.72	96.72	93.8	97.81	97.08	1.82	82.48
	95	98.18	98.91	96.35	96.35	98.18	96.72	93.8	93.43	97.08	7.3
A_{G_1}		**93.07**	**94.53**	92.34	**92.34**	87.96	95.62	97.45	98.18	98.18	92.7

semi-aware TD- and BU- DJCD, we used the optimal feature dimensions in the latent low-dimensional space equal to $d_r^{\mathrm{TD}} = 200$ and $d_r^{\mathrm{BU}} = 60$, respectively. Table 10 reports performance metrics of different methods on CCID database in the quantization-semi-aware scenario. The highlighted values in the bold type represent the best score. As it can be seen, the proposed algorithms show better performance in comparison with methods [7, 18, 31] in the quantization-semi-aware scenario.

Table 8: The detection accuracies of the proposed BU learning strategy on original raw CCID database in terms of percentage

A_{G_2}		l_1									
		50	55	60	65	70	75	80	85	90	95
l_2	50	**47.08**	**97.45**	**98.18**	**98.91**	**99.64**	**100**	**98.54**	**98.18**	**97.81**	**97.08**
	55	**98.54**	**47.45**	**99.27**	**99.27**	**98.91**	**98.91**	**99.27**	**97.81**	**98.91**	**94.89**
	60	**100**	**97.81**	**46.35**	**99.27**	**99.64**	**99.64**	**100**	**98.18**	**99.27**	**97.45**
	65	**100**	**99.64**	**99.64**	**44.16**	**100**	**99.64**	**100**	**100**	**97.81**	**97.81**
	70	**100**	**100**	**99.64**	**99.64**	**45.26**	**99.64**	**99.64**	100	**99.27**	**97.81**
	75	**100**	**100**	**100**	**100**	**99.27**	**47.45**	**100**	**100**	99.27	**98.91**
	80	**100**	**100**	**100**	**100**	100	**100**	**55.11**	**100**	99.64	**100**
	85	99.64	99.27	99.27	**99.64**	**99.64**	100	100	**46.35**	100	100
	90	**100**	**99.64**	**100**	**100**	**100**	100	100	100	**52.92**	**100**
	95	99.64	100	100	**100**	100	**100**	100	100	100	**39.42**
A_{G_1}		53.28	52.55	52.92	55.47	55.84	52.19	44.89	51.82	44.16	50

Table 9: The detection accuracies of our combined TD/BU approach on original raw CCID database in terms of percentage

A_{G_2}		l_1									
		50	55	60	65	70	75	80	85	90	95
l_2	50	10.95	84.31	90.15	97.45	90.88	99.64	97.08	89.42	89.05	78.47
	55	89.78	15.69	88.69	93.43	91.24	83.58	84.31	87.59	97.81	79.56
	60	97.45	90.88	20.07	95.62	95.99	90.15	98.54	94.53	95.99	91.61
	65	98.54	96.35	94.89	15.69	95.62	90.51	98.18	99.27	85.04	86.13
	70	98.18	99.27	98.91	94.16	21.90	95.99	96.35	**100**	**99.64**	89.78
	75	99.27	99.64	99.27	99.64	90.15	18.25	97.45	97.81	97.08	92.70
	80	98.91	98.54	99.64	99.27	**100**	99.27	17.15	98.18	**99.64**	97.45
	85	**100**	**99.64**	**100**	98.54	99.27	**100**	**100**	17.15	**100**	**100**
	90	98.91	99.27	99.27	98.91	99.27	**100**	**100**	**100**	20.80	99.64
	95	**100**	**100**	**100**	99.64	**100**	99.64	**100**	**100**	**100**	8.76
A_{G_1}		89.05	84.31	80.29	84.31	78.10	82.12	83.21	81.02	77.01	91.61

3.3 Identification efficiency of recompression history

3.3.1 Performance with quantization-unaware scenario

As mentioned in Section 2.2.1, the proposed BU-DJCD approach can be also employed to explicitly identify quantization history. Therefore, we gained the learned BU classifier in Section 3.2.1. Table 11 lists the quantization-unaware estimation error of the primary and secondary compression's quality levels by

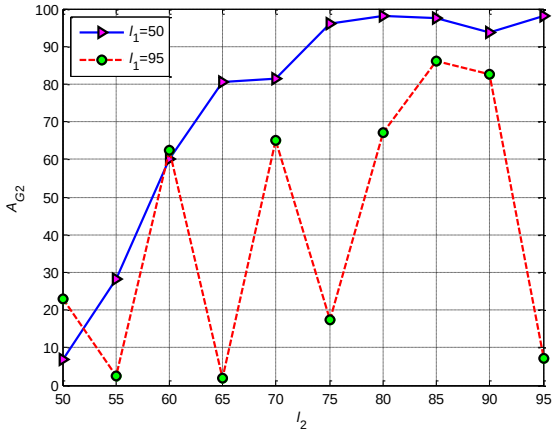

(a)

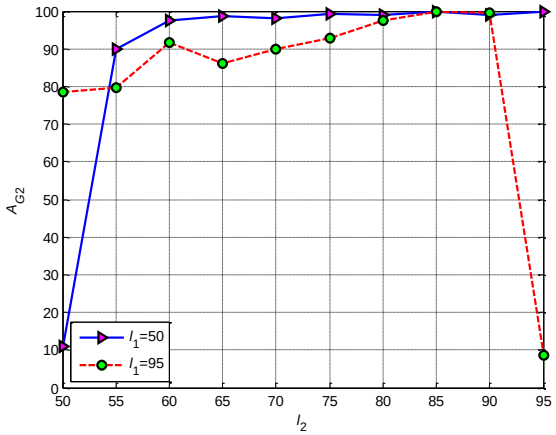

(b)

Fig. 8: The accuracy percentage of double compression detection, A_{G_2}, in terms of l_2 for $l_1 = 50, 95$ pertaining to (a) the TD learning strategy, which this strategy alone is even more effective than the competing methods [7, 18, 31], and (b) the perceptual TD/BU approach. In Fig. 8 (a), the periodic and unstable behavior for the curve with $l_1 = 95$ is completely obvious; whereas our combined scheme compensates this defect. Please note that starting and ending points of curves are belonging to the exception case of $l_1 = l_2$.

Table 10: Performance metrics of different approaches on CCID database for the quantization-semi-aware double JPEG compression detection in terms of percentage

Method	Performance metrics							
	Sensitivity				Specificity	Accuracy	G-mean	F_1-measure
	$l_1 < l_2$	$l_1 = l_2$	$l_1 > l_2$	Total				
B. Li et al. method [18]	99.81	30	98.14	92.08	95.88	93.98	93.96	93.86
Milani et al. method [31]	94.17	25.91	73.53	78.05	85.93	81.99	81.90	81.25
Dong et al. method [7]	99.71	22.96	97.58	91.07	**96.45**	93.76	93.72	93.59
Proposed TD strategy	99.73	28.21	98.67	92.1	96.31	94.21	94.18	94.08
Proposed BU strategy	99.62	**43.25**	98.92	**93.67**	95.00	94.34	94.33	94.30
Proposed combined TD/BU approach	**99.82**	35.29	**99.16**	93.07	96.13	**94.60**	**94.59**	**94.52**

Table 11: The quantization-unaware estimation error of the primary and secondary compression's quality levels via the proposed BU learner. E_{G_1} and E_{G_2} denote estimation errors for G_1 and G_2 groups in percentage, respectively.

E_{G_2}		l_1									
		50	55	60	65	70	75	80	85	90	95
l_2	50	61.31	5.47	2.92	3.28	3.28	0.36	2.55	4.01	4.74	6.93
	55	4.38	59.85	3.65	3.28	2.55	2.92	3.65	2.92	2.55	8.39
	60	1.09	3.28	60.22	1.46	2.19	2.92	2.19	3.28	2.55	5.84
	65	0.73	1.09	1.09	62.04	2.55	1.09	0.36	0.73	5.11	5.84
	70	2.19	1.09	1.09	1.09	57.66	2.92	1.82	0	2.19	6.93
	75	1.82	1.82	1.09	2.19	2.19	57.66	1.09	0.73	2.55	3.65
	80	1.46	1.46	1.46	1.46	1.09	0.36	46.35	1.09	0.36	1.09
	85	1.82	1.82	1.09	1.46	1.09	0.36	0	53.65	0	0
	90	1.09	2.19	2.19	0	0.36	0	0	0	47.08	0
	95	0.73	0.73	0	0.36	0.36	0	0	0	0	60.58
E_{G_1}		56.2	51.82	49.64	49.64	48.18	50.36	55.11	48.54	55.84	50

the proposed BU approach on testing-set originated from raw CCID database. In this table, E_{G_1} and E_{G_2} denote estimation errors for G_1 and G_2 groups in terms of percentage, respectively. As it is shown, for doubly JPEG compressed images, the results are very promising especially in cases for which $l_1 \neq l_2$. Please note that the cause of random guess for quantization-unaware estimating l_1 in a single compressed image is its misclassification error as a double compressed one with $l_2 = l_1$, which is related to the nature of the proposed features.

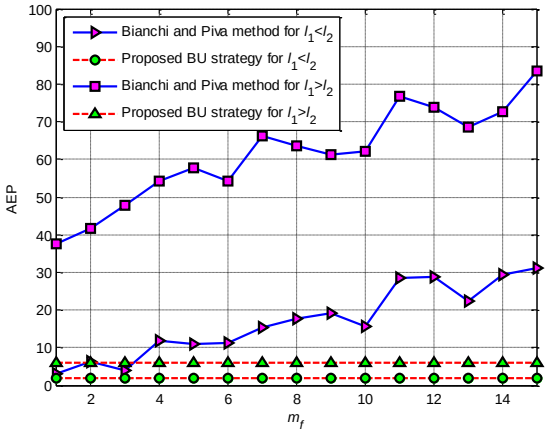

Fig. 9: The Average Error Percentage (AEP) in terms of the first 15 frequency modes of Bianchi and Piva method, and the proposed BU strategy for all $l_1 < l_2$ and $l_1 > l_2$ from all images.

3.3.2 Performance with quantization-semi-aware scenario

In this experiment, at first, we trained the proposed quantization-semi-aware BU-DJCD method on whole single and double compressed JPEG images created by CCID database. Afterwards, to validate the parameters, test and compare, we provided another database including fully double compressed JPEG images created by RCID image-set. Total test samples were $100 \times 208 = 20800$ images. Then, we fed these test images to the suggested primary quantization table estimator as well as the competing Bianchi and Piva approach [3] in the same baseline coding conditions.

To assess the effectiveness of the aforementioned methods, we determined the average percentage of erroneously estimated quantization steps for each $(l_1,\ l_2)$ introduced in [12]. Fig. 9 compares the Average Error Percentage (AEP) in terms of the frequency modes, m_f, sorted in a zig-zag order defined in JPEG compression standard [45] for all $l_1 < l_2$ and $l_1 > l_2$ from all test images. The error curves for estimating the first quantization matrix demonstrate that the proposed BU quantization estimator is more accurate than those of Bianchi and Piva method, relative to different frequency modes. The robust and stable behavior of the quantization steps estimation in terms of m_f is also obvious. Other benefit of our method is to accurately estimate the whole of the first quantization matrix entries. However, the method of [3] is fragile to estimate the entries corresponding to middle and high frequencies in the baseline quantizer.

3.4 Real image forgery detection tests

In this experiment, we have investigated the performance of the proposed quantization-semi-aware TD, BU and combined TD/BU approaches to JPEG image forgery detection. Here, we utilized two different databases, i.e. NCID for training and CCID for testing purposes. To provide small information-rich image patches for training, at first, we divided each raw image of NCID database into four quartile patches with the equal dimensions of 128×128. This operation creates $4 \times 5150 = 20600$ image patches, from which 5150 candidate samples were randomly selected as a new raw database. Afterwards, this database is completely employed to create different types of single and double compressed images in order to train the models of the proposed TD and BU approaches. In the learning phase, for PCA dimensionality reduction technique, we estimated the optimal reduced feature dimensions for TD and BU strategies as $d_r^{\mathrm{TD}} = 100$ and $d_r^{\mathrm{BU}} = 50$, respectively.

In order to evaluate, we considered a kind of real manipulations in which an object from an uncompressed image is inserted into a singly compressed JPEG image with the compression's quality level l_1. The composite image is resaved in the same JPEG format with the compression's quality level l_2, for which the foreground, i.e. the inserted object, and background areas undergo single and double compression, respectively. As mentioned, this kind of tampered JPEG images were provided via CCID database. In this experiment, we set the experimental parameters $l_1 = 50$ and $l_2 = 85$. Some examples to demonstrate the effectiveness of the proposed combined TD/BU approach for locating tampered regions are portrayed in Fig. 10.

To figure out the localization efficiency of tampered regions, we utilized a performance measure similar to one introduced in [40]. In our problem, the probability of error for a localized tampered image may be defined as

$$P_e \triangleq 1 - \frac{A\left(\mathbf{G} \cap \mathbf{F}\right)}{A\left(\mathbf{G} \cup \mathbf{F}\right)}, \tag{14}$$

in which $\mathbf{G}$ denotes the ground truth binary image, and the operator $A\left(\cdot\right)$ calculates the area. In fact, this definition gives an error measure of aligning or overlapping between the ground truth data and the segmented image $\mathbf{F}$.

We also compared localization results of the proposed TD, BU and combined TD/BU tampering detection approaches with those of the algorithm [19]. For a fair comparison, we trained the algorithm [19] to the same database as well as the parameter settings used in our tests. Table 12 reports the error characteristics of the proposed approaches as well as the competing method. In this table, $\mu_{\mathbf{P}_e}$ and $\sigma_{\mathbf{P}_e}$ respectively represent the sample's mean and standard deviation of the vector $\mathbf{P}_e$ encompassing the probability of error for all tested images. The error percentage characteristics show the proposed perceptual TD/BU approach outperforms other state-of-the-art methods to locate the tampered regions of JPEG images. In the application of forgery detection, although, the error characteristics of the proposed BU algorithm are more than

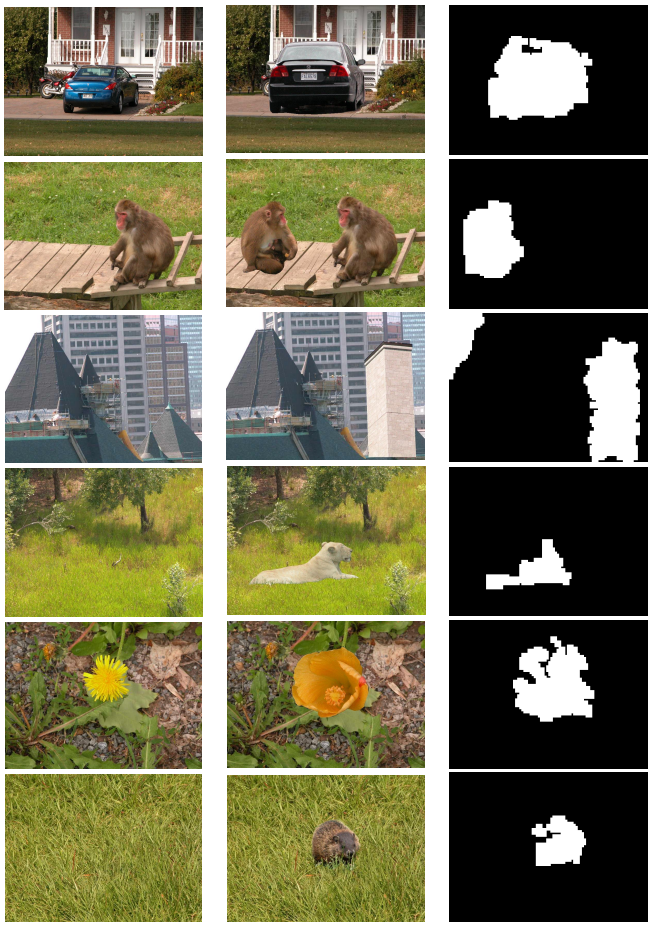

(a) (b) (c)

Fig. 10: The application of the proposed combined TD/BU approach to real-world forensic investigations including (a) original images, (b) tampered images, and (c) image forgery segmented results.

our TD learning strategy, it is better to localize foreground tampered objects in images rather than detecting background accurately.

4 Discussion and conclusion

This paper introduced a novel and robust forensic image analysis tool in order to discover the traces left by double JPEG compression. Briefly, the proposed technique can answer the following questions with and without knowing the quantization table information.

Table 12: The error percentage characteristics of the proposed forgery localization approaches against the competing method of [19]

Method	Error characteristics	
	$\mu_{\mathbf{P}_e}$	$\sigma_{\mathbf{P}_e}$
Algorithm [19]	13.68	8.56
Proposed TD strategy	7.66	7.15
Proposed BU strategy	8.62	8.40
Proposed combined TD/BU approach	5.90	5.62

1. Is the suspect image an original single JPEG compressed one or has it undergone the compression twice?
2. What is the primary compression history of a previously double JPEG compressed image?
3. Which regions of the questionable JPEG image have borne double compression?

In the identification pipeline, we first proposed a dimensionality reduction algorithm dedicated to the information visualization task. Our visualizer consists of a combination of linear and non-linear schemes which discovers the complex structure of single/double compressed data better than the modern techniques. In this context, the big-data analysis of various singly and doubly compressed JPEG images with different compression's quality levels generated valuable knowledge which led to designing a robust learning strategy for detecting the clues of double JPEG compression in digital images.

Then, we described the perceptual idea behind the bottom-up, top-down and combined top-down/bottom-up learning strategies and empirically demonstrated their significant superiority compared to other state-of-the-art related approaches. We also showed that the proposed learning strategy is robust to some extent than the competitors. It is because our technique considers the local and global structures among various types of singly and doubly compressed data. The results revealed that utilizing coder information and behavior for discovering double compression traces can considerably improve the performance in comparison to other methods. This intuition may encourage a trend toward advising source coder-specific mechanisms to approach an appropriate court-friendly performance.

In order to cover all species of S/D compression for industrial applications, i.e. $\forall l_1, l_2 \in \{1,\ 2,\ \ldots, 100\}$, we suggest two alternatives. The first option is to utilize generative models like distance-based approaches, which are often employed in visual recognition tasks, to be able to encompass all types. In the second solution, we are pursuing an intermediate learning strategy as a variant of the proposed BU style in which all double compression kinds are grouped into three abstract categories, namely classes pertaining to $l_1 < l_2$, $l_1 = l_2$ and $l_1 > l_2$ parts. Hence, for such a learning strategy, the number of classes to exclusively detect double compression will reduce to four classes, i.e. one class belonging to single compression group and others for double compression.

For the considered scenario of forgery in the paper, an object from a raw image is inserted into an original single compressed image and is compressed again in the JPEG format. In this case, the resulting forged image experiences exactly an aligned DCT grid at two successive compression stages. However, if we first crop the original JPEG image and then insert the object into it and/or paste an object from a singly compressed JPEG image to a raw image and finally recompress as JPEG, the probability of grid alignment will equal to $\frac{1}{64}$ in average. These types of tampering cause background and/or foreground areas to misclassify. It means that we cannot successfully separate real forged regions, i.e. the inserted object. Therefore, the proposed method fails in such a new scenario. Now, as a future research opportunity, we are aiming to consider these kinds of image forgery in our detector.

Specifically, this work can be developed for accurate detecting of double JPEG compression in the case $l_2 = l_1$. Throughout the paper, the proposed approach addressed the JPEG image compression scheme. As a further research opportunity, we recommend the generalization of the proposed detection pipeline as a generic model to other compression standards like JPEG 2000 (JP2) and Google Web Picture (WebP), for identifying their related recompression traces.

Acknowledgment

The authors would like to thank S. Sabouri for her valuable comments which help us to improve the quality of this paper.

References

1. Baudat, G., Anouar, F.: Generalized discriminant analysis using a kernel approach. Neural Computation **12**(10), 2385–2404 (2000)
2. Berger, A., Hill, T.P.: A basic theory of Benford's law. Probability Surveys **8**, 1–126 (2011)
3. Bianchi, T., Piva, A.: Image forgery localization via block-grained analysis of JPEG artifacts. IEEE Transactions on Information Forensics and Security **7**(3), 1003–1017 (2012)
4. Borenstein, E., Ullman, S.: Combined top-down/bottom-up segmentation. IEEE Transactions on Pattern Analysis and Machine Intelligence **30**(12), 2109–2125 (2008)
5. Chang, C.C., Lin, C.J.: LIBSVM: a library for support vector machines. ACM Transactions on Intelligent Systems and Technology (TIST) **2**(3), article 27 (2011)
6. Cheng, H., Liu, Z., Yang, L., Chen, X.: Sparse representation and learning in visual recognition: theory and applications. Signal Processing **93**(6), 1408–1425 (2013)

7. Dong, L., Kong, X., Wang, B., You, X.: Double compression detection based on Markov model of the first digits of DCT coefficients. In: IEEE 6th International Conference on Image and Graphics (ICIG), pp. 234–237 (2011)
8. Duarte, M.F., Eldar, Y.C.: Structured compressed sensing: from theory to applications. IEEE Transactions on Signal Processing **59**(9), 4053–4085 (2011)
9. Evans, N., Bozonnet, S., Wang, D., Fredouille, C., Troncy, R.: A comparative study of bottom-up and top-down approaches to speaker diarization. IEEE Transactions on Audio, Speech, and Language Processing **20**(2), 382–392 (2012)
10. Farid, H.: Digital image ballistics from JPEG quantization. Tech. Rep. TR2006-583, Department of Computer Science, Dartmouth College (2006)
11. Farid, H.: Image forgery detection. IEEE Signal Processing Magazine **26**(2), 16–25 (2009)
12. Galvan, F., Puglisi, G., Bruna, A., Battiato, S.: First quantization matrix estimation from double compressed JPEG images. IEEE Transactions on Information Forensics and Security **9**(8), 1299–1310 (2014)
13. Gao, J., Shi, Q., Caetano, T.S.: Dimensionality reduction via compressive sensing. Pattern Recognition Letters **33**(9), 1163–1170 (2012)
14. He, H., Garcia, E.A.: Learning from imbalanced data. IEEE Transactions on Knowledge and Data Engineering **21**(9), 1263–1284 (2009)
15. Jolliffe, I.T.: Principal component analysis. Springer Series in Statistics, The 2nd edition (2002)
16. Kaski, S., Peltonen, J.: Dimensionality reduction for data visualization. IEEE Signal Processing Magazine **28**(2), 100–104 (2011)
17. Levin, A., Weiss, Y.: Learning to combine bottom-up and top-down segmentation. International Journal of Computer Vision **81**(1), 105–118 (2009)
18. Li, B., Shi, Y.Q., Huang, J.: Detecting doubly compressed JPEG images by using mode based first digit features. In: IEEE 10th Workshop on Multimedia Signal Processing, pp. 730–735 (2008)
19. Li, X.H., Zhao, Y.Q., Liao, M., Shih, F.Y., Shi, Y.Q.: Detection of tampered region for JPEG images by using mode-based first digit features. EURASIP Journal on Advances in Signal Processing pp. 1–10 (2012)
20. Lin, H.T., Lin, C.J., Weng, R.C.: A note on Platt's probabilistic outputs for support vector machines. Machine learning **68**(3), 267–276 (2007)
21. Lin, W.S., Tjoa, S.K., Zhao, H.V., Liu, K.R.: Digital image source coder forensics via intrinsic fingerprints. IEEE Transactions on Information Forensics and Security **4**(3), 460–475 (2009)
22. Lin, Z., He, J., Tang, X., Tang, C.K.: Fast, automatic and fine-grained tampered JPEG image detection via DCT coefficient analysis. Pattern Recognition **42**(11), 2492–2501 (2009)
23. Liu, J., Ji, S., Ye, J.: SLEP: sparse learning with efficient projections. Arizona State University (2011) (2011)

24. Liu, Q., Sung, A.H., Qiao, M.: A method to detect JPEG-based double compression. In: The 8th International Conference on Advances in Neural Networks, Lecture Notes in Computer Science, Part II, pp. 466–476 (2011)
25. Liu, Q., Sung, A.H., Qiao, M.: Neighboring joint density-based JPEG steganalysis. ACM Transactions on Intelligent Systems and Technology (TIST) **2**(2), article 16 (2011)
26. Lukáš, J., Fridrich, J.: Estimation of primary quantization matrix in double compressed JPEG images. In: Proc. Digital Forensic Research Workshop (2003)
27. van der Maaten, L.: Learning a parametric embedding by preserving local structure. In: International Conference on Artificial Intelligence and Statistics, pp. 384–391 (2009)
28. van der Maaten, L., Hinton, G.: Visualizing data using t-SNE. Journal of Machine Learning Research **9**, 2579–2605 (2008)
29. van der Maaten, L., Postma, E.O., van den Herik, H.J.: Dimensionality reduction: a comparative review. Tech. Rep. TiCC-TR 2009-005, Tilburg Centre for Creative Computing, Tilburg University (2009)
30. Mahalakshmi, S.D., Vijayalakshmi, K., Priyadharsini, S.: Digital image forgery detection and estimation by exploring basic image manipulations. Digital Investigation **8**(3), 215–225 (2012)
31. Milani, S., Tagliasacchi, M., Tubaro, S.: Discriminating multiple JPEG compression using first digit features. In: IEEE International Conference on Acoustics, Speech and Signal Processing (ICASSP), pp. 2253–2256 (2012)
32. Olmos, A., Kingdom, F.A.A.: A biologically inspired algorithm for the recovery of shading and reflectance images. Perception **33**(12), 1463–1473 (2004)
33. Pearson, K.: On lines and planes of closest fit to systems of points in space. Philosophical Magazine **2**(11), 559–572 (1901)
34. Peng, Y., Liu, B.: Accurate estimation of primary quantisation table with applications to tampering detection. Electronics Letters **49**(23), 1452–1454 (2013)
35. Piva, A.: An overview on image forensics. ISRN Signal Processing p. article ID 496701 (2013)
36. Redi, J.A., Taktak, W., Dugelay, J.L.: Digital image forensics: a booklet for beginners. Multimedia Tools and Applications **51**(1), 133–162 (2011)
37. Sencar, H.T., Memon, N.: Identification and recovery of JPEG files with missing fragments. Digital Investigation **6**, S88–S98 (2009)
38. Silverman, B.W.: Density estimation for statistics and data analysis. Monographs on Statistics and Applied Probability **26**, 1–22 (1986)
39. Soille, P.: Morphological image analysis: principles and applications. Springer-Verlag New York, Inc. , The 2nd edition (2004)
40. Taimori, A., Behrad, A.: A new deformable mesh model for face tracking using edge based features and novel sets of energy functions. Multimedia Tools and Applications **74**(23), 10,735–10,759 (2015)

41. Taimori, A., Razzazi, F., Behrad, A., Ahmadi, A., Babaie-Zadeh, M.: A proper transform for satisfying Benford's law and its application to double JPEG image forensics. In: IEEE International Symposium on Signal Processing and Information Technology (ISSPIT), pp. 000,240–000,244 (2012)
42. Taimori, A., Razzazi, F., Behrad, A., Ahmadi, A., Babaie-Zadeh, M.: Quantization-unaware double JPEG compression detection. Journal of Mathematical Imaging and Vision (2015). DOI 10.1007/s10851-015-0602-z
43. Tian, H., Fang, Y., Yao, Z., Lin, W., Ni, R., Zhu, Z.: Salient region detection by fusing bottom-up and top-down features extracted from a single image. IEEE Transactions on Image processing **23**(10), 4389–4398 (2014)
44. Ulusoy, I., Bishop, C.M.: Generative versus discriminative methods for object recognition. In: IEEE Computer Society Conference on Computer Vision and Pattern Recognition (CVPR), vol. 2, pp. 258–265 (2005)
45. Wallace, G.K.: The JPEG still picture compression standard. IEEE Transactions on Consumer Electronics **38**(1), xviii–xxxiv (1992)